Chemical Science

ROYAL SOCIETY OF CHEMISTRY

EDGE ARTICLE

View Article Online
View Journal | View Issue

Cite this: *Chem. Sci.*, 2026, **17**, 3278

All publication charges for this article have been paid for by the Royal Society of Chemistry

Modulating resonance structures toward highly efficient violet-blue organic light-emitting diodes with narrow emission

Xinyu Wang, Hanlin Gan, Mingliang Xie, Wenle Tan, Pengfei Niu, Mingke Li, Xinru Liao, Bohan Wang, Lei Ying, Yue Yu * and Yuguang Ma

Received 26th September 2025
Accepted 11th December 2025

DOI: 10.1039/d5sc07474f

rsc.li/chemical-science

The spectral narrowing of organic fluorescence materials is a focus issue in the field of photochemistry and organic light-emitting diodes (OLEDs). Donor–acceptor emitters are usually susceptible to environmental interference, exhibiting significant spectral broadening. However, as the energy of the donor and acceptor is matched, a resonant energy form is formed in the molecule, resulting in a narrower and stronger spectrum. The resonance structures of such emitters can be evaluated by the resonance parameter c^2. When the neutral state and zwitterionic state of dye molecules are in equilibrium, $c^2 = 0.5$, and this state is called the cyanine limit state. Here, we introduce DOBNA-carbazole-based donor–acceptor emitters BO-2Cz and TB-tCz. The c^2 value of BO-2Cz (0.45) indicates that BO-2Cz has a more balanced contribution of resonance structures than TB-tCz (0.03). Although both exhibit short-wavelength emission with small full width at half maximum (FWHM) in *n*-hexane, TB-tCz shows significant spectral broadening in different solvents and the doped film, while BO-2Cz maintains narrow violet-blue emission with high environmental tolerance. As a result, the single-doped device with BO-2Cz achieves electroluminescence at 404 nm (FWHM = 31 nm), CIE coordinates (0.162, 0.017), and a maximum external quantum efficiency of 7.3%, simultaneously realizing short-wavelength and narrow emission.

Introduction

Organic light-emitting diode (OLED) materials that combine high efficiency with small full-width at half maximum (FWHM) are pivotal to achieving wide color gamuts and low energy consumption in future ultra-high-definition displays.[1,2] The donor–acceptor (D–A) structural design strategy stands as an effective approach to developing high-performance emitters.[3–5] The difficulty lies in the fact that the spectra of D–A structured molecules are prone to broadening due to the energy mismatch between the donor and the acceptor, making them highly sensitive to environmental factors (*e.g.*, solvents, hosts, aggregation).[6,7] It was found that for low-dimensional charge-transfer state fluorescence dyes, modulation of the molecule's resonance forms *via* its donors and acceptors enables the achievement of stable, narrow spectra. Take the classic narrow-emission dye cyanine as an example, it can be described as the resonance hybrid of a neutral (N) structure and a charge-separated zwitterionic (Z) structure according to a simple two-state model. For these dyes, electron density is transferred from the HOMO (predominantly localized in the donor region) to the LUMO (mainly confined to the acceptor region). To the first approximation, the excited state of these molecules can be approximated as a radical cation/anion pair.[8] According to Mulliken theory,[9] the ground-state ($\Psi_{NZ}(S_0)$) and excited-state wavefunctions ($\Psi_{NZ}(S_1)$) can be described as a linear combination of the neutral (N) wavefunction (Ψ_N) and the zwitterionic (Z) wavefunction (Ψ_Z). The contribution of the two resonance structures strongly depends on the strength of the electron-donor and electron-acceptor groups.[10–14] Upon introducing c to represent the fraction of the Z structure in the molecular wavefunction, the expressions for the wavefunctions of the dye's ground state (S_0) and first excited state (S_1) can be formulated, as presented in eqn (1) and (2).[15]

$$\Psi_{NZ}(S_0) = c\Psi_Z - (1 - c^2)^{0.5}\Psi_N \quad (1)$$

$$\Psi_{NZ}(S_1) = c\Psi_N + (1 - c^2)^{0.5}\Psi_Z \quad (2)$$

As seen in Fig. 1, when c^2 is 0, the resonance structure of the molecule belongs to the N resonance. At a value of 1, it is dominated by the Z structure. At this point, cyanine dyes exhibit a broad spectrum due to the significant structural difference between $S_0$and S_1. When the c^2 is 0.5, the wavefunctions of the N and Z resonance structures contribute equally to the molecule's overall wavefunction. Since this situation naturally exists in symmetric cyanine dyes, it is sometimes referred to as the

Guangdong Basic Research Center of Excellence for Energy and Information Polymer Materials, State Key Laboratory of Luminescent Materials and Device, South China University of Technology, Guangzhou 510640, P. R. China. E-mail: yuyue924@scut.edu.cn

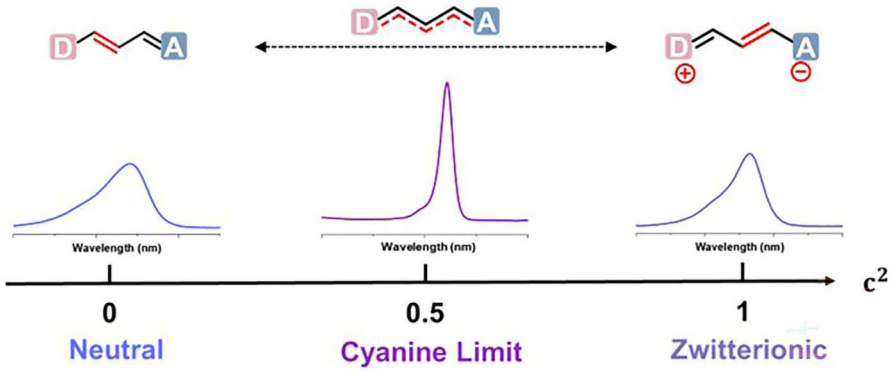

Fig. 1 The c^2 values and absorption spectra of the neutral, cyanine limit, and zwitterionic structures in cyanine dyes.

"cyanine limit". In this state, the overlap between the electron-vibrational wavefunctions of $S_0$and $S_1$is maximal, and high-frequency vibrations (such as C–C bond stretching vibration) during molecular excitation can be effectively suppressed, showing strong and narrow spectral characteristics. Hush *et al.* derived the soliton solution for cyanine dyes through the SSH model, proving that cyanine dyes exhibit soliton electronic structure characteristics.[16–19] Consequently, cyanine dyes exhibit soliton characteristics: bond length equalization and alternating distribution of positive and negative charges. As a self-reinforcing isolated wave, soliton can maintain its own characteristics without being affected by the environment. It has its own characteristics without being affected by the environment. It has been proven that many dyes with soliton characteristics exhibit solvent insensitivity.[20]

In D–A type fused-ring fluorescent molecules, researchers have similarly observed that the spectral properties of the molecules are closely associated with their resonance states, and stable spectral narrowing can be achieved through the modulation of D/A units.[21] Multiple resonance thermally activated delayed fluorescence (MR-TADF) materials exemplified by boron–nitrogen materials can effectively suppress structural relaxation and achieve narrow emission by introducing electron-donating and electron-accepting heteroatom pairs at appropriate positions in fused-ring aromatics.[22–25] DOBNA, the first oxygen-containing MR ultraviolet emitter, was created by replacing N atoms with O atoms, which have a weaker electron-donating ability.[26] Subsequently, using DOBNA as the acceptor unit, researchers have developed numerous D–A structured molecules, aiming to realize efficient short-wavelength narrow emission materials. While short-range and long-range CT excited states have already been employed to account for these phenomena in studies of MR materials, we seek to revisit these spectral behaviors from the perspective of resonance state structural modulation, drawing upon the model of cyanine dyes. Here, we synthesized two emitters named BO-2Cz and TB-tCz based on the DOBNA as the acceptor and carbazole as the donor, which exhibit different environmental resistance capabilities due to variations in resonance structures. The resonance forms in the two emitters have been proved by the c^2 value. The c^2 value of TB-tCz is 0.03, while that of BO-2Cz is 0.45, indicating that the two resonance structures in BO-2Cz contribute more evenly. By comparing the film spectra and solvation effect spectra of the two emitters, it is confirmed that BO-2Cz has better environmental resistance and can maintain its narrow-emission spectral characteristics. The EL peak of the doped device based on BO-2Cz is located at 404 nm, with a FWHM of 31 nm. The corresponding CIEy value reaches 0.017, and the maximum external quantum efficiency (EQE_{max}) is 7.3%, which is one of the highest values at the violet-blue color gamut. It proves that modulating the resonance structure enables short-wavelength and narrow emission, and the resonance structures can be measured using the c^2 value.

Results and discussion

The specific molecular structures are shown in Fig. 2a. TB-tCz is obtained by the Vilsmeier–Haack coupling reaction of *tert*-butylcarbazole and DOBNA-Br in an alkaline environment. BO-2Cz is obtained by the Suzuki reaction of the boronic acid pinacol ester on the B2Cz and the Br atom on DOBNA-Br. The synthetic routes for TB-tCz and BO-2Cz are illustrated in Schemes S1 and S2. Both TB-tCz and BO-2Cz are D–A structured molecules composed of DOBNA and carbazole derivative groups. The main difference is that BO-2Cz has an additional benzene ring between the donor and acceptor groups, adopting a meta-conjugation, which is a key factor for resonance. The final products are characterized by ^{1}H NMR and ^{13}C NMR in Fig. S1–S4. Their ^{1}H NMR and ^{13}C NMR show that all the obtained substances were pure target products.

The photophysical, thermodynamic, and electrochemical properties of these two emitters are listed in Table 1. Both TB-tCz and BO-2Cz exhibit excellent thermal stability, with decomposition temperatures (T_d) of 396 °C and 490 °C in Fig. S5, respectively. Theoretical calculations on the ground and excited states of TB-tCz and BO-2Cz were performed based on density functional theory (DFT) at the BMK-D3(BJ)/6-311G(d,p) theoretical level. The analyses of hole–electron distributions were finished by Multiwfn, and the isosurfaces were rendered by the VMD program.[27–29] Additional details on calculations and information about instrumentation are provided in SI S1. The cyclic voltammetry measurements revealed that the highest

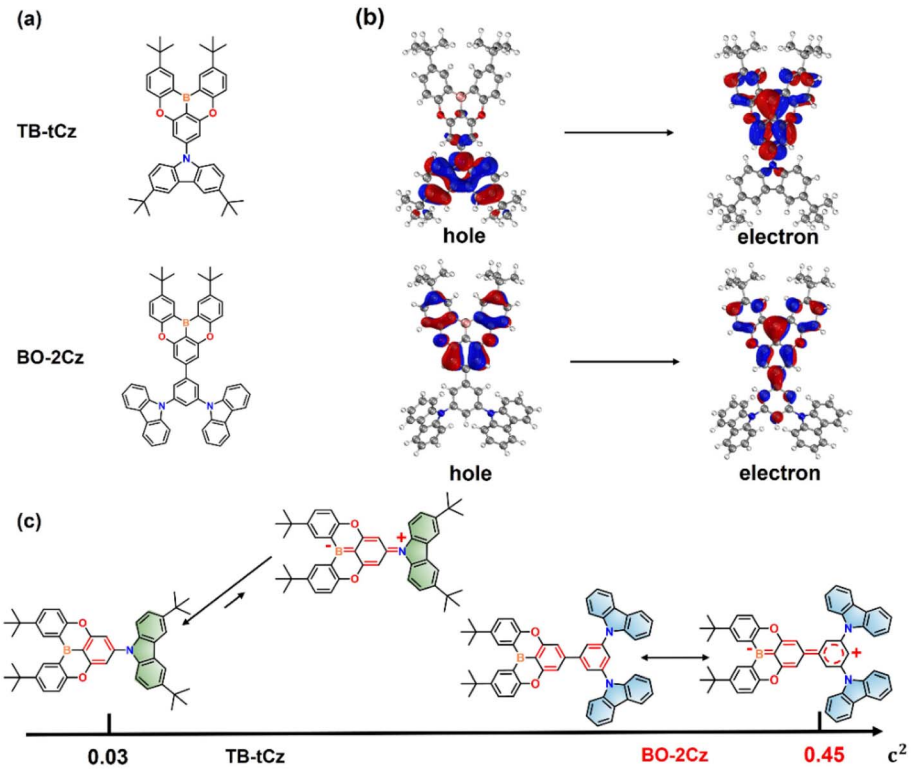

Fig. 2 (a) The structures of TB-tCz and BO-2Cz; (b) the NTOs of TB-tCz and BO-2Cz; (c) the c^2 value and the resonance structures of TB-tCz and BO-2Cz.

occupied molecular orbital (HOMO) energy levels of TB-tCz and BO-2Cz are −5.50 eV and −5.67 eV, and the lowest unoccupied molecular orbital (LUMO) energy levels are −3.64 eV and −3.50 eV, respectively. The CV curves are listed in Fig. S6. The frontier orbital distributions of TB-tCz and BO-2Cz are listed in Fig. S7. Both materials show a certain degree of overlap but partial separation in their frontier orbital distributions, exhibiting hybridized local and charge transfer (HLCT) characteristics.[30–32] The reorganization energies and Huang-Rhys factors of the two emitters are presented in Fig. S8. TB-tCz and BO-2Cz exhibit nearly identical reorganization energies, which aligns well with their similar frontier orbital distributions, further corroborating their analogous transition mechanisms. Specifically, BO-2Cz demonstrates a lower reorganization energy of 3256.9 cm^{-1} compared to TB-tCz's 3694.1 cm^{-1}, suggesting a smaller configurational difference between its ground and excited states. Since resonance structures are closely linked to the photophysical properties of molecules, describing the resonance structures of molecules is beneficial for understanding their spectral behaviors. In this work, we attempt to use the numerical value of c^2 as a metric for the mixing of the N and Z structures to measure the relative weight of the two resonance forms in the molecule: c^2 is 0 for the pure N structure, 0.5 at the cyanine limit, and 1 for the pure Z structure. Consequently, the closer c^2 is to 0.5, the more balanced the contributions of the two structures to the ground state, leading to molecules exhibiting stable narrow spectra.[33] According to the literature, the c^2 value can be calculated using eqn (3):

$$c^2 = 1/2[1 - \Delta\mu(4\mu_{ag}{}^2 + \Delta\mu^2)^{-1/2}] \quad (3)$$

which μ_{ag} represents the transition dipole moment, $\Delta\mu$ represents the dipole change upon optional excitation ($\Delta\mu = \mu_a - \mu_g$). The data could be obtained through theoretical calculations, and the c^2 will be obtained by substituting the data into the

Table 1 Summary of the photophysical, thermal, and electrochemical properties of TB-tCz and BO-2Cz

Emitters	$\lambda_{abs}{}^a$ [nm]	$\lambda_{em}{}^b$ [nm]	FWHM [nm eV^{-1}]	Φ^d [%]	τ^d [ns]	T_d [°C]	HOMO/LUMO [eV]
TB-tCz	368[c]	387[c]/402[d]	16/0.09[c] 40/0.30[d]	54.1	4.38	396	−5.50/−3.64
BO-2Cz	389[c]	402[c]/408[d]	18/0.14[c] 32/0.23[d]	46.2	6.54	490	−5.67/−3.50

[a] The maximum of absorption peaks. [b] The maximum of photoluminescent peaks. [c] Measured in *n*-hexane (1×10^{-5} M). [d] Measured in films (1 wt% doped in CzSi).

Table 2 The computational dipole moment of ground states ($|\mu_g|$) and excited state ($|\mu_a|$), the transition dipole moment ($|\mu_{ag}|$), oscillator strength (f_{osc}), and energy (E_{ag}) of the $S_1 \rightarrow S_0$ process[a]

Emitter	$\|\mu_g\|$/debye	$\|\mu_a\|$/debye	$\|\mu_{ag}\|$/debye	f_{osc}	E_{ag}/eV	Expt/eV	c^2
TB-tCz	2.321	20.208	3.164	0.192	3.34	3.20	0.03
BO-2Cz	3.297	3.995	3.301	0.160	3.14	3.08	0.45

[a] The gas-phase geometry, dipole moment of S_1 and S_0, and transition dipole moment of the $S_1 \rightarrow S_0$ process are obtained at the BMK-D3(BJ)/6-311G(d,p) theoretical level. The transition energy and oscillator strength of the $S_1 \rightarrow S_0$ process are evaluated at the TD-SCS-ωPBEPP86/6-311G(d,p) level using the BMK-D3(BJ) optimized geometry.

formula. The results of TB-tCz and BO-2Cz are listed in Table 2. The comparison of relevant calculation methods is listed in Table S1. By comparing the calculation results with the experimental results, the BMK-D3(BJ)/6-311G(d,p) theoretical level for theoretical calculation is finally determined. The cartesian coordinates of the S_0 state and S_1 state of TB-tCz and BO-2Cz are listed in Tables S2–S5.

As depicted in Fig. 2c, TB-tCz exhibits a c^2 value of 0.03, suggesting that its molecular structure is predominantly governed by the N structure, with negligible contribution from the Z structure. In contrast, the c^2 value of BO-2Cz nearing 0.5 demonstrates an almost equal contribution from both N and Z structures. At this point, the structure of BO-2Cz is closer to the cyanine limit than that of TB-tCz, which confers enhanced resistance of its spectrum to changes in the external environment. As shown in Table 2, the significant difference of the c^2 stems from the distinction in the excited-state dipole moments between these two emitters. According to the natural transition orbitals (NTOs) calculated in Fig. 2b, for TB-tCz, holes are predominantly distributed on the carbazole groups, while electrons are mainly localized on the boron-oxygen core. This spatial separation of holes and electrons is characteristic of a CT state transition. For BO-2Cz, both holes and electrons are primarily distributed across the boron-oxygen core and the central benzene ring, indicating that BO-2Cz exhibits a localized transition characteristic. Since TB-tCz belongs to the CT transition, its excited-state dipole moment is significantly larger than that of BO-2Cz, resulting in a smaller structural difference between the S_0 and S_1. Thus, the c^2 of TB-tCz is smaller than that of BO-2Cz. This difference is closely related to the resonance structures of molecules.

The differences in resonance state structures are manifested in spectral behaviors, and the degree of prominence of such differences varies across diverse environments. The steady-state photophysical behaviors of TB-tCz and BO-2Cz in *n*-hexane solutions and doped films were investigated using UV-vis absorption (Abs) and photoluminescence (PL) spectroscopy at room temperature. As shown in Fig. 3a and b, in low-polarity *n*-hexane (HEX) solution, TB-tCz and BO-2Cz exhibit distinct absorption bands at 368 nm and 389 nm. For PL spectra, TB-tCz and BO-2Cz display similar violet-blue sharp emission, peaking at 387 nm and 402 nm, with a FWHM of 16 nm and 18 nm, respectively. Notably, both emitters exhibit extremely narrow emission, displaying characteristics of the cyanine limit. This confirms that the two resonance structures of both materials contribute in a relatively balanced manner, likely because the emission of both emitters in low-polarity solvents is dominated by the local-state emission of DOBNA. Since the host material forms a highly polar environment that can affect the photophysical properties of the emitters, we further investigated the steady-state photophysical properties of the emitters in doped films (1 wt% doped in CzSi). Unlike the similar spectral behaviors exhibited in *n*-hexane, their film spectra exhibit marked discrepancies. Under the influence of the host material, the emission spectrum of TB-tCz in the doped film exhibits a red shift and broadening: its FWHM increases to 40 nm, and the peak position shifts red to 402 nm. Compared with TB-tCz, BO-2Cz displays a more stable emission spectrum, with a FWHM of 32 nm and a peak position of 408 nm, indicating that its spectrum is less susceptible to environmental effects. This characteristic is closely related to the equal contribution of the two resonance structures.

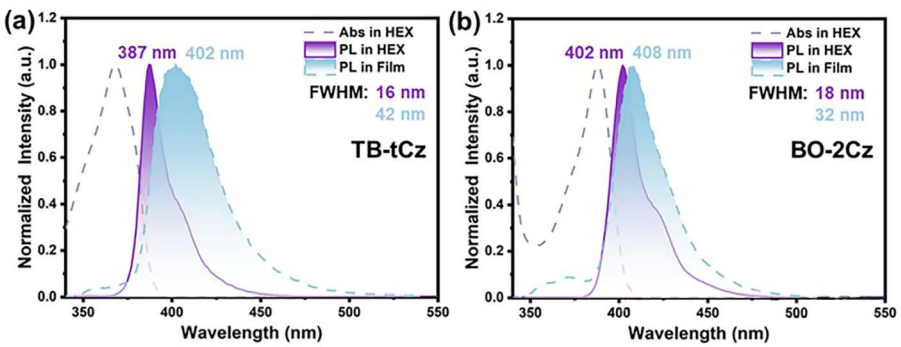

Fig. 3 The Abs and PL spectra of TB-tCz (a) and BO-2Cz (b) in *n*-hexane and the film.

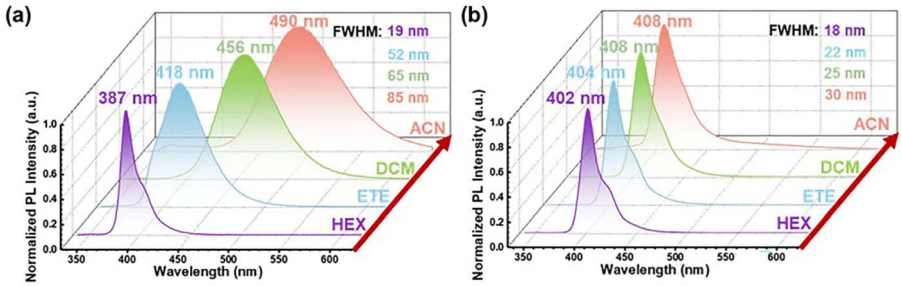

Fig. 4 The PL spectra of TB-tCz (a) and BO-2Cz (b) in different solvents (1×10^{-5} M).

Solvatochromism experiments further reflect the relationship between the strength of resonance structure coupling and the environmental sensitivity of the spectrum. As shown in Fig. 4, we measured the solvation effect on the PL spectra of TB-tCz and BO-2Cz. Four solvents were selected: *n*-hexane (HEX), diethyl ether (ETE), dichloromethane (DCM), and acetonitrile (ACN), ordered by increasing polarity in Fig. 4a and b. With the increase of solvent polarity, the emission of the TB-tCz solution shows an obvious bathochromic shift and broadening: the peak position shifts from 386 nm in HEX to 490 nm in ACN, and the FWHM expands from 16 nm to 85 nm. In contrast, BO-2Cz exhibits considerable stability. The peak position of the PL spectrum only moved about 6 nm from HEX (402 nm) to ACN (408 nm), and the FWHM changed from 18 nm in HEX to 30 nm in ACN. This arises from the differing strengths of resonance state coupling between the two emitters. In the low-polarity environment, the energies of the resonance states of TB-tCz and BO-2Cz are comparable, both displaying the characteristics of the cyanine limit. For TB-tCz with weak resonance-state coupling, increasing solvent polarity leads to a divergence in the energies of its two resonance states, resulting in spectral broadening. This behavior is consistent with CT-state transitions and matches the theoretical calculations. The stronger CT state character of TB-tCz causes the energy of its Z-type resonance state to decrease rapidly in high-polarity solvents, thereby weakening the resonance state coupling between N and Z. BO-2Cz, with the stronger resonance-state coupling, exhibits stronger soliton-like electronic structure characteristics than TB-tCz, such as more uniform bond lengths and more balanced charge magnitudes, in Fig. S9. Consequently, the spectrum of BO-2Cz exhibits excellent environmental robustness.

BO-2Cz retains its short-wavelength and narrow-spectrum properties in the doped film, highlighting its promising potential for achieving high-color-purity violet-blue

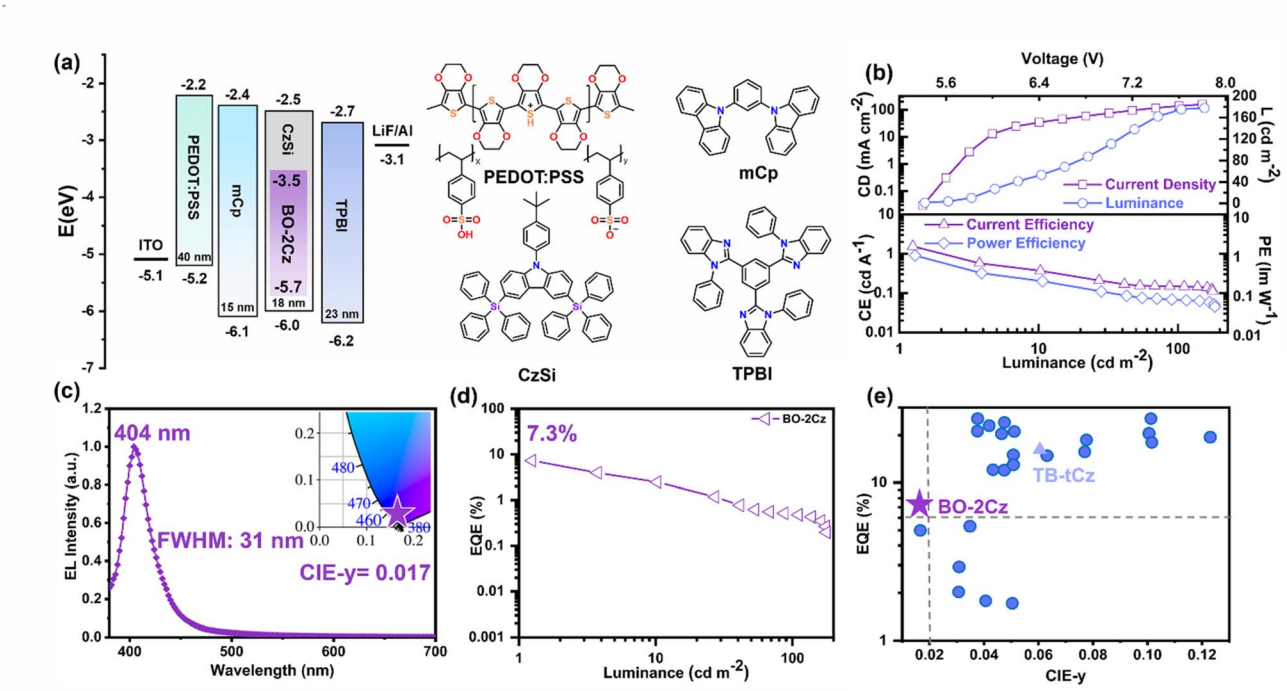

Fig. 5 (a) The energy level diagram and the structures of functional layer materials in the OLED; (b) the current density–voltage–luminance (*J*–*V*–*L*) and the current efficiency–luminance–power efficiency (CE–L–PE) curves of BO-2Cz; (c) the normalized electroluminescence spectra and the CIE coordinates of BO-2Cz OLED; (d) The efficiency–luminance (EQE–L) curve of BO-2Cz; (e) The comparison of the device properties between BO-2Cz and the devices that have been reported.

electroluminescence. Additionally, the photoluminescence quantum yields (PLQY) of TB-tCz and BO-2Cz doped films reach 54.1% and 46.2%, respectively. Low-temperature fluorescence and phosphorescence spectra of the two emitters were recorded at 77 K, as presented in Fig. S10. Comparison with the spectrum of TB-tCz reveals that BO-2Cz exhibits a larger singlet-triplet energy gap, which is consistent with the theoretically calculated energy levels shown in Fig. S11. Transient fluorescence spectroscopy measurements detected no long-lived signals on the microsecond (μs) timescale, further ruling out the possibility of a TADF mechanism (see Fig. S12). Given the HLCT excited-state characteristics of BO-2Cz, it holds potential as a hot exciton material.[34,35]

To evaluate its electroluminescent properties, BO-2Cz was used as a guest material for fabricating binary-doped devices. The performance of the OLED based on BO-2Cz is presented in Fig. 5. The structure of the OLED is ITO/PEDOT: PSS (40 nm)/mCp (15 nm)/CzSi: 1 wt% BO-2Cz (18 nm)/TPBI (23 nm)/Li (1 nm)/Al (100 nm), with the chemical structures of PEDOT: PSS, mCp, CzSi, and TPBI also depicted in Fig. 5a. In this OLED device, PEDOT: PSS, mCp, CzSi, and TPBI serve as the hole injection layer, hole transport layer, host material in the emitting layer, and electron transport layer, respectively. The maximum luminance is approximately 177 cd m^{-2}. The current efficiency–luminance–power efficiency (CE–L–PE) curves are presented in Fig. 5b, and the corresponding maximum current efficiency and power efficiency are 1.55 cd A^{-1} and 0.90 lm W^{-1}, respectively. Note that owing to its strong soliton-like characteristics, BO-2Cz retains violet-blue emission with a small FWHM in the doped device, thus enabling narrow-band violet-blue electroluminescence. As shown in Fig. 5c, the EL spectrum peak is at 404 nm with a FWHM of 31 nm/0.225 eV.

Additionally, the BO-2Cz-based device achieved an EQE_{max} of 7.3% in Fig. 5d. The properties of these emitters are in Table S3, and the structures are listed in Scheme S3. The corresponding CIEy can reach 0.017, exhibiting extremely high color purity. By contrast, the literature-reported TB-tCz-doped device, constrained by its relatively broad emission spectrum, exhibits a CIEy value of 0.06.[36] By comparing the performance of devices similar to our device, when the EQE of such emitters exceeds 10%, their CIEy values are basically above 0.04.[36] In contrast, for emitters with a CIEy value of less than 0.04, their EQE is generally below 5%.[37] These results demonstrate that our device exhibits high color purity and high EQE in the violet-blue wavelength range. According to the transient electroluminescence (EL) spectrum of BO-2Cz in Fig. S13, the BO-2Cz-based device shows almost no delay and its performance is hardly dependent on the applied voltage, thus ruling out the influence of the triplet–triplet annihilation (TTA) effect on the device. In addition, we have also calculated the exciton utilization efficiency (EUE) of BO-2Cz.[38] Assuming that excitons undergo complete recombination and taking the light extraction efficiency as 20%, the EUE of the device is calculated to be 79%, which exceeds 25% (theoretical EUE_{max} for fluorescence), indicating that it has a more efficient exciton utilization channel. Therefore, BO-2Cz exhibits a hot exciton channel guided by the HLCT excited state.

Conclusions

In summary, two emitters, TB-tCz and BO-2Cz, were successfully synthesized and characterized. In *n*-hexane solution, both emitters exhibited narrow emission in the violet-blue region. Notably, while TB-tCz showed significant spectral broadening in the doped film state, BO-2Cz maintained a narrow emission. This discrepancy can be attributed to the different degrees of energies matching between the donor and the acceptor, causing the difference between the resonance structures, which has been proved by the c^2 value. The c^2 value of BO-2Cz is 0.45, which is closer to 0.5 compared with that of TB-tCz (0.03), indicating that BO-2Cz is closer to the cyanine limit state. Thus, BO-2Cz exhibits enhanced environmental resistance and enables the preservation of its spectral shape and position across different states. As a result, a device fabricated based on BO-2Cz achieved violet-blue electroluminescence at 404 nm with a small FWHM of 31 nm, featuring a remarkable violet-blue color purity of CIEy <0.02. By drawing on the simple two-state model of cyanine dyes, this work provides a novel perspective for understanding the relationship between the spectral properties and structures of materials.

Author contributions

Wang completed the characterization and analysis of the emitters. H. Gan and M. Li completed the DFT calculation. M. Xie performed the device fabrication and electroluminescence analysis. W. Tan assisted in performance analysis. P. Niu synthesized the emitters. X. Liao and B. Wang conducted the electrochemical performance tests. X. Wang and Y. Yu wrote and revised the manuscript. Y. Lei and Y. Ma guided and supervised the entire project. All authors contributed to the general discussion.

Conflicts of interest

There are no conflicts to declare.

Data availability

The data supporting this article and SI have been included as part of the supplementary information (SI). Supplementary information is available. See DOI: https://doi.org/10.1039/d5sc07474f.

Acknowledgements

This work was supported by the National Key R&D Program of China (2020YFA0714604), the National Natural Science Foundation of China (52503365, 92463310), the Guangdong Basic and Applied Basic Research Foundation (2024A1515110241), and the Fund of Guangdong Provincial Key Laboratory of Luminescence from Molecular Aggregates (2023B1212060003).

Notes and references

1 J. Wang, X. Zhai, C. Ji, M. Zhang, C. Yao, G. Xie, J. Zhang and X. Xi, *Dyes Pigment.*, 2023, **219**, 111586.
2 J. Wang, Y. Niu, Y. Jiang, C. Yao, Z. Dai, Y. Deng and J. Zhang, *Chem. Eng. J.*, 2025, **15**, 169199.
3 X. Qiu, S. Xue, Y. Wu, M. Che, Q. Su and W. Yang, *J. Mater. Chem. C*, 2016, **4**, 5988–5995.
4 J. Shi, Q. Din, L. X, X. L, Z. Liu, Q. Su, Y. Pa, S. Xu and W. Yang, *J. Mater. Chem. C*, 2018, **6**, 11063–11070.
5 S. Xu, X. Qi, S. Yin, Y. Lu, Y. Pan, Q. Su, C. Gu and W. Yang, *Adv. Opt. Mater.*, 2017, **5**, 1700747.
6 J. C. Haenle, K. Bruchlos, S. Ludwig, A. Köh and S. Laschat, *Chempluschem*, 2017, **82**, 1197–1210.
7 K. C. Kreß, T. Fischer, J. Stumpe, W. Frey, M. Raith, O. Beiraghi, S. H. Eichhorn, S. Tussetschläger and S. Laschat, *Chempluschem*, 2014, **79**, 223–232.
8 P. Maslak, A. Chopra, C. R. Moylan, R. Wortmann, S. Lebus, A. L. Rheingold and G. P. A. Yap, *J. Am. Chem. Soc.*, 1996, **118**, 1471–1481.
9 S. L. Boyd, R. J. Boyd, Z. Shi, L. R. C. Barclay and N. A. Porter, *J. Am. Chem. Soc.*, 1993, **115**, 682.
10 H. Mustroph, K. Reiner, B. Senns, J. Mistol, S. Ernst, D. Keil and L. Hennig, *Chem.–Eur. J.*, 2012, **18**, 8140–8149.
11 S. V. Shishkina, V. V. Dyakonenko, A. A. Ishchenko and A. V. Kulinich, *Struct. Chem.*, 2021, **33**, 169–178.
12 L. G. S. Brooker, G. H. Keyes, R. H. Sprague, R. H. VanDyke, E. V. L. G. VanZandt, F. L. White, H. W. J. Cressman and S. G. Dent Jr, *J. Am. Chem. Soc.*, 1951, **73**, 5332–5350.
13 S. Dähne, Color and Constitution: One Hundred Years of Research, *Science*, 1978, **199**, 1163.
14 S. Dähne and F. Moldenhauer, Structural Principles of Unsaturated Organic Compounds: Evidence by Quantum Chemical Calculations, *Prog. Phys. Org. Chem.*, 1985, **15**, 1.
15 R. Wortmann, C. Poga, R. J. Twieg, C. Geletneky, C. R. Moylan, P. M. Lundquist, R. G. DeVoe, P. M. Cotts, H. Horn, J. E. Rice and D. M. Burland, *J. Chem. Phys.*, 1996, **105**, 10637–10647.
16 J. S. Craw, J. R. Reimers, G. B. Bacskay, A. T. Wong and N. S. Hush, *Chem. Phys.*, 1992, **167**, 101–109.
17 J. S. Craw, J. R. Reimers, G. B. Bacskay, A. T. Wong and N. S. Hush, *Chem. Phys.*, 1992, **167**, 77–99.
18 W. P. Su, J. R. Schrieffer and A. J. Heeger, *Phys. Rev. Lett.*, 1979, **42**, 1698–1701.
19 W. P. Su, J. R. Schrieffer and A. J. Heeger, Soliton excitations in polyacetylene, *Phys. Rev. B:Condens. Matter Mater. Phys.*, 1980, **22**, 2099–2111.
20 W. Tan, Y. Yu, T. Shi, L. Zhang, H. Gan, B. Wang, G. Liu, M. Li, L. Ying and Y. Ma, *Adv. Mater.*, 2024, **36**, 2410418.
21 W. Tan, Y. Yu, Y. Li, H. Gan, L. Xu, M. Li, B. Wang, L. Wang, X. Wang, L. Ying and Y. Ma, *Angew. Chem., Int. Ed.*, 2025, **64**, e202500235.
22 Y. Kondo, K. Yoshiura, S. Kitera, H. Nishi, S. Oda, H. Gotoh, Y. Sasada, M. Yanai and T. Hatakeyama, *Nat. Photonics*, 2019, **13**, 678–682.
23 S. Oda, W. Kumano, T. Hama, R. Kawasumi, K. Yoshiura and T. Hatakeyama, *Angew. Chem., Int. Ed.*, 2021, **60**, 2882–2886.
24 K. Stavrou, S. M. Suresh, D. Hall, A. Danos, N. A. Kukhta, A. M. Z. Slawin, S. Warriner, D. Beljonne, Y. Olivier, A. Monkman and E. Zysman-Colman, *Adv. Opt. Mater.*, 2022, **10**, 2200688.
25 M. Yang, I. S. Park and T. Yasuda, Full-Color, *J. Am. Chem. Soc.*, 2020, **142**, 19468–19472.
26 H. Hirai, K. Nakajima, S. Nakatsuka, K. Shiren, J. Ni, S. Nomura, T. Ikuta and T. Hatakeyama, *Angew. Chem., Int. Ed.*, 2015, **54**, 13581–13585.
27 W. Humphrey, A. Dalke and K. Schulten, VMD: Visual molecular dynamics, *J. Mol. Graph.*, 1996, **14**, 33.
28 T. Lu and F. Chen, *J. Comput. Chem.*, 2012, **33**, 580.
29 T. Lu and F. Chen, *J. Theor. Comput. Chem.*, 2012, **11**, 163.
30 L. Yao, Y. Pan, X. Tang, Q. Bai, F. Shen, F. Li, P. Lu, B. Yang and Y. Ma, *J. Phys. Chem. C*, 2015, **119**, 17800–17808.
31 W. Li, Y. Pan, R. Xiao, Q. Peng, S. Zhang, D. Ma, F. Li, F. Shen, Y. Wang, B. Yang and Y. Ma, *Adv. Funct. Mater.*, 2014, **24**, 1609–1614.
32 W. Li, Y. Pan, L. Yao, H. Liu, S. Zhang, C. Wang, F. Shen, P. Lu, B. Yang and Y. Ma, *Adv. Opt. Mater.*, 2014, **2**, 892–901.
33 F. Würthner, C. Thalacker, R. Matschiner, K. Lukaszuk and R. Wortmann, *Chem. Commun.*, 1998, **16**, 1739–1740.
34 L. Yao, S. Zhang, R. Wang, W. Li, F. Shen, B. Yang and Y. Ma, *Angew. Chem., Int. Ed.*, 2014, **53**, 2119–2123.
35 Y. Pan, W. Li, S. Zhang, L. Yao, C. Gu, H. Xu, B. Yang and Y. Ma, *Adv. Opt. Mater.*, 2014, **2**, 510–515.
36 H. J. Kim, H. Kang, J. Jeong, S. H. Park, C. W. Koh, C. W. Kim, H. Y. Woo, M. J. Cho, S. Park and D. H. Choi, *Adv. Funct. Mater.*, 2021, **31**, 2102588.
37 Z. Zhao, C. Zeng, X. Peng, Y. Liu, H. Zhao, L. Hua, S. J. Su, S. Yan and Z. Ren, *Angew. Chem., Int. Ed.*, 2022, **61**, e202210864.
38 P. Xu, L. Xu, Y. Pan, D. Yang, Z. Ma, X. Qiao, D. Hu, D. Ma and Y. Ma, *J. Mater. Chem. C*, 2022, **10**, 6596–6602.